Soft Matter

A Surface with Stress, Extensional Elasticity, and Bending Stiffness

Journal:	*Soft Matter*
Manuscript ID	SM-ART-01-2019-000075.R1
Article Type:	Paper
Date Submitted by the Author:	28-Mar-2019
Complete List of Authors:	Lapinski, Nicole; Lehigh University P C Rossin College of Engineering and Applied Science, Chemical and Biomolecular Engineering Liu, Zezhou; Cornell University, Department of Mechanical and Aerospace Engineering Yang, Shu ; University of Pennsylvania, Materials Science and Engineering Hui, Chung-Yuen; Cornell University, Theoretical and Applied Mechanics Jagota, Anand; Lehigh University, Bioengineering

A Surface with Stress, Extensional Elasticity, and Bending Stiffness[1]

Nicole Lapinski[1], Zezhou Liu[3], Shu Yang[4], Chung-Yuen Hui[3], Anand Jagota[1,2,*]

[1]Department of Chemical and Biomolecular Engineering and [2]Department of Bioengineering
Lehigh University, Bethlehem PA 18017
[3]Department of Mechanical & Aerospace Engineering, Cornell University, Ithaca, New York
[4]Department of Materials Science and Engineering, University of Pennsylvania, 3231 Walnut Street, Philadelphia, PA 19104

[*] Corresponding Author
Anand Jagota
D331 Iacocca Hall, 111 Research Drive,
Lehigh University
Bethlehem PA 18015 (USA)
anj6@lehigh.edu

Short Title: Surface Stress and Elasticity

[1] Electronic supplementary information (ESI) available. See DOI: ??

ABSTRACT

We demonstrate that the surface of a commonly used polydimethylsiloxane formulation (PDMS, Sylgard 184) treated by ultraviolet ozonolysis (UVO) has significant surface stress, considerable extensional elasticity (the "Shuttleworth Effect"), *and* surface bending elasticity. For soft solids, phenomena such as wetting, contact, surface flattening, and stiffening by liquid inclusions are often governed by their surface, which is usually represented by a liquid-like constant surface stress. Whether the surfaces of soft solids can have more complex constitutive response is actively debated. We studied the deformation of three surface-patterned materials systems: untreated polydimethylsiloxane (PDMS), an organogel, and patterned PDMS with surface treatment by UVO. The last of these three, we found, has complex surface elasticity. This is analogous to the situation for liquids in which the presence of a second phase at the interface yields Gibbs elasticity. Our finding is of broad applicability because in soft solids the behavior of the surface can often dominate bulk deformation.

Keywords: Surface Stress, Elastocapillarity, Surface Elasticity, Soft Materials

1. INTRODUCTION

The importance of *surface energy* (a scalar) for surface phenomena is well established.[1-2] However, a closely related but *different* quantity, *surface stress* (a two-dimensional tensor), has a relatively weak role to play in stiff solids[3]. Its effects are typically felt over a characteristic length scale, the *elastocapillary length*, σ_o/E, where E is the Young's modulus and σ_o is the magnitude of the surface stress. For example, if we attempt to make a sharp edge in a soft elastic solid, say by molding against a sharp corner in a hard material such as silicon, the radius of curvature to which the sharp edge will relax due to surface stress is on the order of the elastocapillary length.[4] For an *isotropic solid surface*, surface stress is an isotropic tensor of magnitude σ_o, which is usually called the *surface tension,* and its value need not be the same as the surface energy of the solid. For conventional stiff materials (*e.g.,* metals and ceramics) the value of elastocapillary length is generally very small, often on the order of Angstroms.[5] Therefore, for conventional engineering materials surface stress effects are felt only at very small length scales such as for small crystals, thin-films, or AFM-cantilevers.[6-10] In comparison, for soft solids such as elastomers and gels with elastic modulus in the MPa to kPa range, respectively, the corresponding value of elastocapillary length is on the order of tens of nanometers to tens of microns or larger.

Thus, for soft materials, surface stress is far more likely to play a significant and sometimes dominant role in surface mechanical phenomena. This, in turn, has sparked a resurgence of interest in this topic.[5] For example, the shape of compliant solid cylinders can spontaneously undulate in a manner analogous to the surface stress driven Rayleigh-Plateau instability of a liquid[11]; surface stress flattens or rounds off sharp edges by deformation.[12-13] The Hertz and Johnson-Kendall-Roberts (JKR) theories for adhesion-less and adhesive contact,[14] respectively, which have been widely used to interpret indentation experiments, may no longer be applicable.[15-19] The contact angle of a liquid drop on a compliant surface is not a material property – it cannot be predicted by Young's equation – but depends on the surface stress of the solid substrate as well as its elasticity.[20-23] The deflection of thin films of relatively stiff materials can be substantially affected by surface stress of the film, which can be exploited to measure solid surface stress.[24-27]

Most recent investigations consider the soft solid surface to have a constant, homogeneous, and isotropic surface stress,[5] which is analogous to the understanding of simple fluid surfaces.[2, 28] For simple single-component fluids, the dominant surface property is a constant surface tension. But, when a strong surfactant adsorbs at the liquid-vapor interface, the complex fluid surface that forms exhibits a full range of rheological behavior.[28] For *solids*, it has long been known that surface stress can be strain dependent.[29] In particular, Gurtin and Murdoch[30] raised the question of whether solid surfaces possess elasticity in addition to a residual surface stress. Gurtin and Murdoch[30] also suggested the possibility that a surface could store energy in bending. However, based on a simple scaling analysis, they concluded that surface extensional and bending elasticity would likely be negligible for simple, single-phase, solids. Steigmann and Ogden extended the Gurtin-Murdoch theory by incorporating bending resistance.[31] This question has not been explored much for soft materials. It has recently been demonstrated experimentally that a surface can have significant extensional elasticity.[32] Another example is the lipid bilayer, which can carry stress and resist bending.[33-35] Another potential example of a surface with constitutive behavior more complex than a simple surface stress is when a thin, partially glassy film forms on the surface of an elastomer upon exposure to oxygen plasma or UV ozone (UVO).[36-39] Elastomer properties are generally affected to depths of a few nm (oxygen plasma) to about 100 nm (UVO).

Thus, in principle, a soft solid surface can have the full complexity of rheological response like the bulk, e.g., surfaces stress, extensional elasticity, bending stiffness, and inelastic behavior. However, there are few studies about when soft surface properties have constitutive behavior more complex than carrying a constant and isotropic surface stress. In this work, we first examine two systems, an organogel and an elastomer, for which it is not necessary to invoke surface elasticity. We then study the deformation of a UVO-treated patterned elastomer in response to its surface stress and applied uniaxial mechanical stretch λ. We show that to capture the deformation of this system can be represented by an elastic surface constitutive response that includes a surface stress, surface extensional elasticity, *and* surface bending stiffness.

2. EXPERIMENTAL

2.1. FABRICATION OF STRUCTURED SURFACES

Surfaces of commercially available poly(dimethylsiloxane) – PDMS (Sylgard 184, Dow Corning) – were patterned with a ridge-channel structure using molds created by photolithographic patterning of a layer of photoresist SU-8 on a silicon wafer (Fig.1 A-D).[13, 40] We report results for geometries with $a = 1.35$ μm and $w = 30$ μm $- 50$ μm (Fig. 1D). A 10:1 weight ratio of PDMS crosslinker to base was mixed by hand. The mixture was degassed under vacuum for 20 min. The mixture was exposed to air and put in vacuum for 10 min, which was repeated two more times until all air bubbles were removed. The mixture was then poured onto the mold and cured at 80°C for 2 h. After cooling to room temperature, the sample was removed from the mold. For the gelatin gel experiments, these patterned PDMS samples were used as molds. A subset of the patterned PDMS samples underwent a 1 h treatment in a UVO cleaner (Model 144AX, Jelight Company, Inc.). It is known[41] that this commercial version of PDMS contains unreacted oligomers that bloom to the surface, and this process can affect properties in a time-dependent manner. One way around this is solvent-extraction of the unreacted oligomers; another is to wait sufficiently long to allow the system to achieve an equilibrium state; we chose the latter. We checked that our experimental results were stable over the duration of the project. For example, PDMS samples including those exposed to UVO and those not, were tested within one day of fabrication and again over a period of a month. Our measurements remained unchanged over this period.

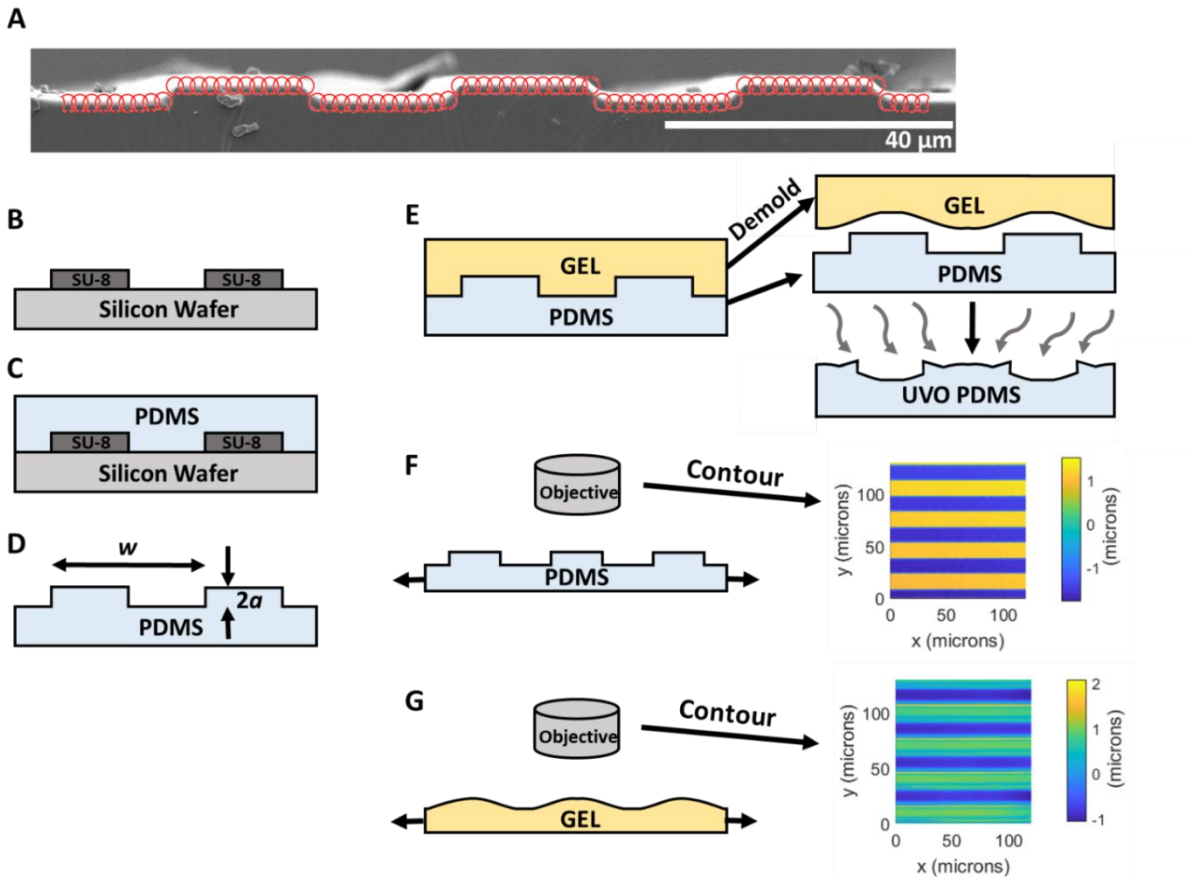

Fig. 1. Schematic illustration of sample fabrication and surface profile measurement. (**A**) A scanning electron microscopy (SEM) image of a PDMS sample with a = 1.35 µm and w = 40 µm. A line scan from the measured surface profile using optical interferometry (*circles)* is overlaid on the SEM micrograph for comparison. Wavelength (w) is the minimum periodic spacing of ridges. Amplitude (a) is half of the ridge height. (**B**) A schematic of the molds created by photolithographic patterning of a layer of SU-8 photoresist on a silicon wafer, (**C**) pouring PDMS onto the silicon wafer mold and, (**D**) removing patterned PDMS after curing. (**E***)* Gel samples were created by replica-molding the gel in the PDMS master from *D*. A set of patterned PDMS samples was further treated by UVO. (**F**,**G**) PDMS and Gel samples were stretched uniaxially and surface profiles were measured for various in-plane stretch values.

2.2. GELATIN GEL FABRICATION

Following the protocol of Paretkar et al.,[13] gelatin-based organogel samples (simply referred to as gels in this work) were fabricated with 10 wt% gelatin dissolved in 70/30 wt% glycerol/water mixture. The gelatin/glycerol/water mixture was continuously stirred at 85°C for 4 h, followed by 1 h degassing (no stirring) at 85°C. The liquid gelatin mixture was poured onto the mold (Fig. 1) and cooled to room temperature for 10 min. The entire assembly was then set at 4°C for 17 h. The gel was placed at room temperature for another 1 h and subsequently demolded.

Each gel sample used for stretching experiments was mounted onto a PDMS backing required for stretching and was molded with a PDMS mold on the top side. This was done by pouring the degassed liquid gelatin mixture into a petri dish between two glass slides with a 610 μm spacer to produce a uniform gel height as shown in Fig. 2*A*. The glass slides, spacers, and PDMS mold were removed leaving a gel structure with a PDMS backing. The excess gel (not molded by the PDMS mold) was removed from the sides by cutting.

2.3. STRETCHING EXPERIMENTS

Stretching experiments were conducted with both the demolded gel on a PDMS backing and the ridge/channel-patterned PDMS with no additional backing. To stretch the samples, the PDMS was clamped onto two aluminum arms attached to a movable stage, as shown in Fig. 2*B*. Using the manipulator, the top stage was moved to stretch the sample. After each stretch the sample was allowed to relax for a few seconds, and the surface profile was measured using a white light interferometric instrument (Zegage; Zygo Corporation). After reaching the maximal stretch desired, the stretch was released in increments and measurements were also made during this unloading process. The first profilometer image taken served as a reference for other images. To align images, each image was rotated so that the ridges/channels ran parallel to the horizontal image axis, and translated to match a chosen reference point on the reference image. Then, a selected portion of the image was analyzed. Typically, 300 – 800 line scans were taken throughout the image, each scan spanning 3-5 ridges. Line scans were analyzed to calculate amplitudes a and wavelengths w and these values were averaged over

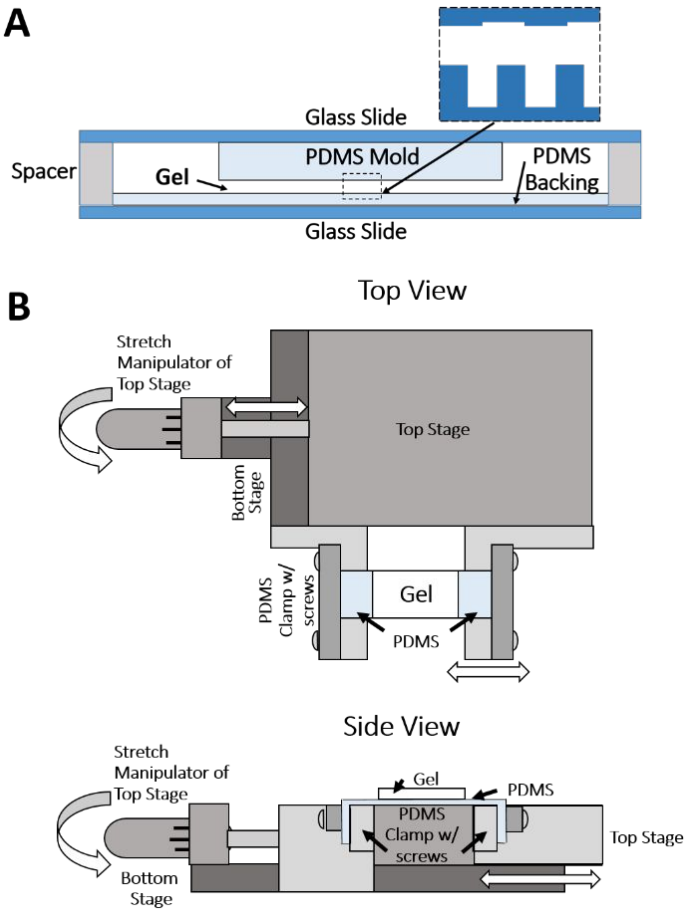

Fig. 2. The experimental setups for gelatin gel molding and sample stretching. (**A**) Illustration of the stretchable gelatin gel molding apparatus, (**B**) Schematic illustration of the PDMS/gel stretching device (top view and side view). The PDMS is clamped onto two aluminum arms attached to a movable stage. A manipulator on the top stage stretches the PDMS base.

all the line scans for a given image.

2.4. YOUNG'S MODULUS (E) MEASUREMENT

In order to determine the Young's modulus, E, of the gel (35.6 ± 1.3 kPa), three indentation experiments were performed and averaged on a gel slab of length L and height h using a custom-built indentation apparatus as in[13]. The gel slab was indented with a cylindrical punch of radius r. For our system $h \gg r$, and in this limit,

$$\lim_{h/r\to\infty}\left(\frac{d\delta}{dP}\right) = C_\infty = \frac{1}{2E^* r} \tag{1}$$

where C_∞ is the compliance, P is the load, δ is the indentation depth, and E^* is the plane strain Young's modulus. $E^* = E/(1-\nu)^2$ relates E^* and E where ν is Poisson's ratio (1/2 for incompressible materials). Combined with the previous equation, this yields

$$E = \frac{3}{8C_\infty a} \tag{2}$$

The indentation experiments produced a linear relationship between the load and indentation depth. The inverse of its slope is C_∞ which was used in Eq. 2 to find E ± standard error. Young's modulus, E, of PDMS was determined by loading flat PDMS sheets of the same thickness as those used in stretching experiments, and taken from the same sample as used in stretching studies, on a rotational rheometer (TA Instrument, ARES-G2) with measurements via a frequency sweep from 0.1 Hz to 100 Hz. Within this range the storage modulus G' is much larger than loss modulus G'' and it varies little with frequency. The average ± standard error values of G' (0.65± 0.01 MPa) was calculated in the low frequency regime (0.1 Hz to 10 Hz). Because PDMS is nearly incompressible, the corresponding value of E=3G' was 1.95 ± 0.03 MPa.

2.5. SIMULATION METHODS

Surface Finite Element. For quantitative interpretation of the experimental data, we implemented a new 3-node surface finite element for nonlinear, implicit, static, 2D plane strain finite element simulations that incorporated surface stretching and bending. Three terms associated with the surface constitute behavior — the zero-strain surface stress σ_0, surface elasticity modulus B, and surface bending stiffness k_b (discussed later) — were required to capture the experimental results. The surface elements, described in more detail in ESI, share surface nodes with continuum finite elements that represent the bulk. Because the bulk elements need only satisfy C_0 continuity, we chose to represent the surface by a set of overlapping 3-node C_0 continuity elements. The kinematic variables, stretch and curvature, were obtained from the geometry information (nodal coordinates) provided by ABAQUS®. Surface contributions to nodal forces and the system Jacobian were derived and computed explicitly, and supplied back to ABAQUS® by writing a user-defined element subroutine. Numerical convergence was ensured by applying the surface stress and surface bending moment incrementally to surface elements.

Finite Element Model: The finite element model is shown schematically in Fig. *3A* and was implemented in ABAQUS®. By symmetry, the width of this model (25μm in Fig. 3*A*) equals half of the wavelength (50μm). The depth was a few times the wavelength. The top flat region occupies one-fourth of the wavelength. The upper corner angle was denoted by θ and measured from SEM images of the cross-section of the sample profile (Fig 1*A*). The values of θ are provided later in Table **1**, along with results, and vary between 120 and 131 degrees. On the left edge, no horizontal displacement or shear traction was allowed; on the bottom edge, the vertical displacement and shear traction were both zero; on the right edge, no shear traction was allowed, and a uniform horizontal displacement field was imposed to simulate the process of stretching. The PDMS/gel was modeled by continuum elements with incompressible neo-Hookean material behavior, and the new surface elements described above were attached to the surface to model the surface constitutive behavior.

Fitting Procedure for Stretching Gel. Straightforward dimensional analysis showed that there is a relationship such that elastocapillary number $\sigma_0 / Ew = f\left(a/w, \lambda\right)$ – both the arguments of the function or the right hand side are measured experimentally. By running over 2000 FEM simulations, we obtained a contour map reflecting this relationship in Fig. 3*B*. Using a 2D cubic spline to interpolate the data, we extracted the surface stress at each experimental data point. With a least-squares fitting of these data we obtained an estimate of the surface stress, and we used this value to make a prediction about the normalized amplitude versus stretch. Data were extracted and analyzed using codes written in Python® and Matlab®.

Fitting Procedure for Stretching UV Ozone Treated PDMS. We allow the surface stress, extensional elasticity, and bending elasticity to vary along the surface. That is, they can be functions of the arc length s along the surface (in the reference configuration; $s = 0$ at the middle point O of the top flat region, see Fig. 3A). We began with the fit by neglecting bending and using the contours in Fig. 3*B* to make a first estimate of the surface stress at each data

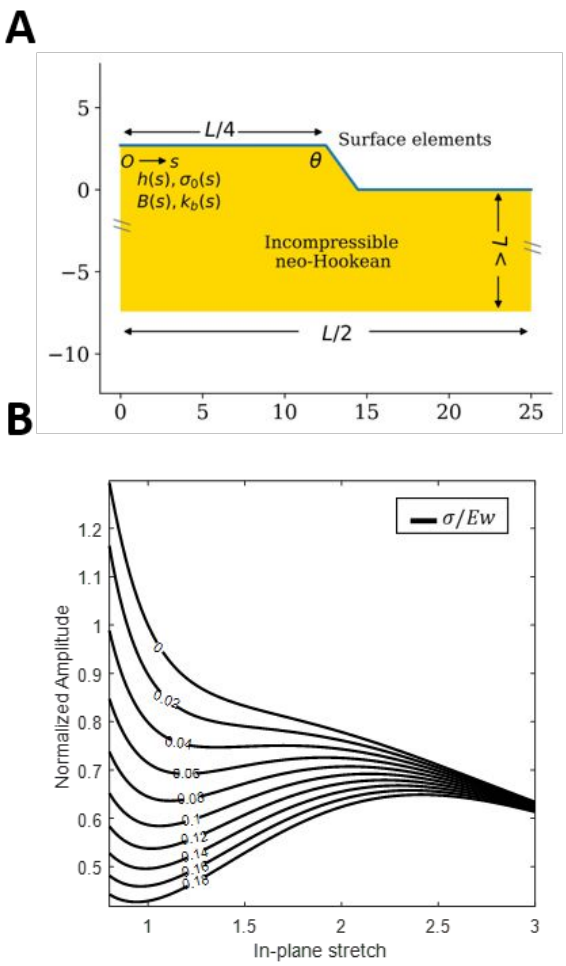

Fig. 3. FEM model schematic and contour of in-plane stretch, normalized amplitude, and elastocapillary number. (**A**) A schematic of FEM model (using the ridge/channel PDMS with $w = 50\ \mu m$ as an example). The new surface elements (solid blue line) were attached to the bulk elements (yellow region), modeled as an incompressible neo-Hookean material. Surface properties were parametrized by the arc length s along the surface starting from the point O. (**B**) Contour plot of relationship between in-plane stretch, normalized amplitude and elastocapillary number (σ_0/Ew).

point. We then fitted experimental data by varying the surface stress $\sigma_0(0)$ and extensional elasticity modulus $B(0)$. Specifically, for the case of 50-micron UVO treated PDMS sample this estimate was $\sigma_0(0) \approx 2.0\,\text{N/m}$ and $B(0) = 20\,\text{N/m}$ (see *ESI*). Next, we used the following iterative method to determine the value of $h(0)$ that best fitted the data: (1) based on the observations of Mills et al., we set the initial value of $h(0)$ = 100nm. (2) Using this value of $h(0)$, we determined the surface thickness profile $h(s)$ by solving a diffusion equation (See ESI for details). Knowing this surface profile completely determined the surface model properties for the FE surface elements. (3) Next, we carried out FE simulations to obtain the change in amplitude and surface profile shape during deformation. (4) We compared the FE results to the experimental data. If the FE results matched both the amplitude change and surface profile details, we exited the iteration; otherwise, we updated the value of $h(0)$ and repeated steps (2) to (4).

3. RESULTS & DISCUSSION

We conducted experiments on three types of surface-patterned samples. One type consisted of PDMS (Young's modulus E=1.95 MPa) with shallow surface ridge-channel patterns, wavelength (w) of 30-50 microns, and amplitude (a) of 1.35 microns, molded from a patterned Si master (Fig. 1*A*-*D*). Another sample type comprised a gelatin-based organogel replica-molded from sample set 1 (Fig. 1*E*). The last sample type was created by exposing some samples from set 1 to UV Ozone for 60 min (Fig. 1*E*). The surface profiles of all samples were measured by white light optical interferometry while subjecting them to varying uniaxial stretch (Fig. 1*F*-*G*). Our previous studies, conducted without uniaxial stretch, showed that the difference in shape of a sample and its mold is the result of deformation caused by surface stress.[13] By mechanically stretching the sample and measuring the resulting change of surface shape, we extended the technique to study surface elasticity. Here, we mechanically applied an incremental in-plane stretch λ perpendicular to the channel length to a maximum value of 10% - 24% (depending on the sample type). We then released the stretch in steps.

3.1. Stretching Untreated PDMS

The untreated patterned PDMS samples were intended to serve as negative controls. For the PDMS we used, elastocapillary length σ_o/E is in the tens of nanometers whereas pattern wavelengths are in tens of microns. Therefore, we expected little effect of surface stress, even if it increased significantly due to stretch. That is, for unstretched samples the surface profile should have faithfully replicated the mold within the resolution of the optical technique used. Moreover, change in the surface profile upon stretching of the sample should have been relatively minor and explainable using bulk elasticity.

Fig. 4*A* shows typical line scans of the stretched and unstretched PDMS and gels. (Results in Figs 4 and 5 are shown for a single representative sample each.) The unstretched patterned PDMS (a = 1.35 μm and w= 50 μm) faithfully replicated the mold shape. Note in particular that the tops of ridges are quite flat. As this sample was stretched, we observed a small but significant change in shape with a characteristic dip in the line scan at the center of each ridge (Fig. 4*A*). Correspondingly, we observed a modest reduction in pattern amplitude of about 5% as shown in Fig. 4*B*. We note that the change in amplitude was the same on loading and unloading – it depended only on the in-plane stretch as expected for an elastic material. This case served as a negative control in that surface stress, surface extensional elasticity, and surface bending are all negligible.

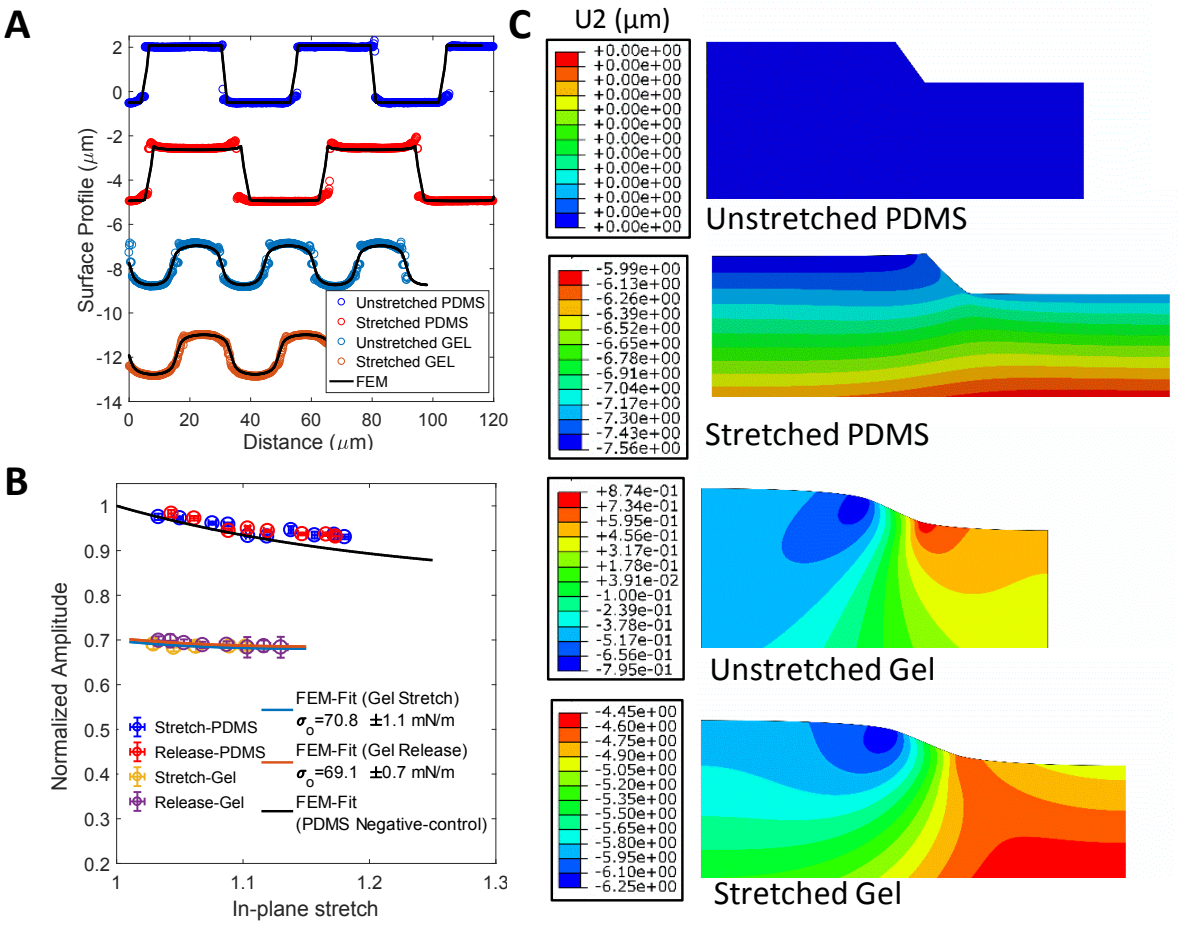

Figure. 4. Results of stretching experiments on the two control systems, untreated PDMS and gelatin gel, with and without stretching. The PDMS sample was constructed from a mold with a = 1.35 μm and w = 50 μm, and the gel sample was constructed from a mold with a = 1.35 μm and w = 30 μm. (**A**) Line scans for the PDMS and gelatin gel in the unstretched and maximum stretched states and their corresponding FEM-predicted results. (**B**) Amplitude normalized by the unstretched PDMS amplitude versus in-plane stretch. Note that for the gelatin gel there is considerable reduction in amplitude due to the effects of surface stress, σ_0. FEM results show that a constant, homogeneous, and strain-independent value of surface stress is sufficient to match experimental measurements. (**C**) Contours of vertical displacement (U2) for four cases, untreated and unstretched PDMS, untreated and stretched PDMS, unstretched gel, and stretched gel.

3.2. Stretching the Gelatin Replica.

The second sample set, comprising patterned gelatin, had a much lower value of Young's modulus, $E \sim 35\ kPa$, and consequently a larger elastocapillary length, on the order of microns. Following Paretkar et al.,[13] gel samples were fabricated by molding into patterned PDMS as shown in Fig. 1. When the cured sample was removed from its mold, the surface deformed to a rounded shape with significantly reduced amplitude (Fig. 4*A,B*). As previously reported,[28] this change of shape could be modeled accurately as deformation driven by a constant surface stress σ_0

$$\frac{a}{a_m} = \frac{8}{\pi}\sum_{n=1}^{\infty} \frac{\sin\left[\frac{(2n-1)\pi}{2}\right]}{(2n-1)\left(1+4\pi\frac{\sigma_0(2n-1)}{wE^*}\right)} \quad (3)$$

where a_m is the mold ridge-channel amplitude and E^* is the plane strain Young's modulus of the gel. When $\sigma_0 = 0$, Eq. 1 is just the Fourier series representation of the undeformed surface profile. Note that the deformed amplitude depends on the dimensionless elastocapillary number $\frac{\sigma_0}{wE^*}$ and higher Fourier modes (larger *n*) decay faster than lower ones. Thus, the gel surface profile had a smaller amplitude and a characteristic wave-like shape with rounded corners (Fig. 4*A*). To explore the effects of in-plane stretch, we stretched the sample in a similar fashion to sample set 1. Figure 4B shows that although the normalized amplitude of surface features, a/a_m, decreased by about 30% to 0.7 (a big change), it showed only a modest (and reversible) further decrease in value with increasing stretch, to a value of no smaller than 0.69 at 10% strain or 110% stretch.

Figs 4*A-B* also show that we can match the deformed surface profile and how it changes with stretch using an FEM model that incorporates a constant, homogeneous, surface stress σ_0. From Fig. 4*B*, we determined $\sigma_0 = 70.8 \pm 1.1$ mN/m during stretching and $\sigma_0 = 69.1 \pm 0.7$ mN/m during stretch release, where the uncertainty in estimated surface stress is based on the uncertainty in measured gel modulus. Thus, this gel system served as a second control.

Fig. 4*C* shows typical contours of computed vertical displacement (U2) for the two control samples, with and without applied stretch. The displacement profile for the stretched PDMS showed approximately uniform vertical strain except near the corners. The displacement profile for the unstretched gel showed high gradients near where the surface curvature was largest, indicating that deformation was driven by surface stress. The displacement profile for the stretched gel can be viewed approximately as a superposition of the stretched PDMS and the unstretched gel.

3.3. Surface Constitutive Model

Before discussing experimental results for the third material system, we introduce the constitutive model framework we propose to use. Based on the fact that the response to stretching in the previous two samples was reversible (and anticipating that this would remain true for the third sample set), we proposed an elastic surface model whose free energy potentially contains contributions from three surface effects: a zero-strain surface stress, surface extensional elasticity, and surface bending elasticity. Specifically, the surface free energy density (per unit area in reference configuration), *A*, of the elastic surface can be described by the Cosserat surface theory.[42] Assuming isotropy and plane strain deformation, A, up to an arbitrary constant, depends on two scalar invariants of the deformation, J_s and $(\kappa - \kappa_o)$ and takes the from

$$A = \sigma_0 (J_s - 1) + \frac{B}{2}(J_s - 1)^2 + \frac{k_b}{2}(\kappa - \kappa_o)^2. \quad (4)$$

Here J_s is the ratio of deformed and undeformed area, given in terms of the surface deformation gradient, $\mathbf{F}_s$, by $J_s = \det(\mathbf{F}_s)$.[30] The term $(\kappa - \kappa_o)/2 = \mathrm{tr}(\boldsymbol{\kappa})/2$ represents the difference between the deformed and initial mean curvatures of the surface where $\boldsymbol{\kappa}$ is the relative curvature tensor associated with the reference configuration. In Eq. 4, σ_0 is the zero-strain surface stress, B is a surface elasticity modulus, and k_b is the surface bending modulus. Eq. 4 is equivalent to the free energy model proposed by Milner et al.[35]

Taking appropriate derivatives of the free energy – see *ESI* and refs[42-44] – we show that under plane strain deformation the surface stress σ_0 and surface bending moment $\mathbf{m}$ in the deformed configuration are related to the local stretch λ_s by

$$\begin{aligned} \boldsymbol{\sigma} &= \left[\sigma_0 + B(\lambda_s - 1)\right]\mathbf{s} \\ \mathbf{m} &= -\lambda_s k_b (\kappa - \kappa_o)\mathbf{s} \end{aligned} \tag{5}$$

where $\mathbf{s}$ is the unit tangent vector of the surface in the deformed configuration, and λ_s is the in-plane stretch. For small deformations, Eq. 5 can be rewritten as

$$\begin{aligned} \boldsymbol{\sigma} &= (\sigma_0 + B\varepsilon_s)\mathbf{s} \\ \mathbf{m} &= -k_b (\kappa - \kappa_o)\mathbf{s} \end{aligned} \tag{6}$$

where ε_s is the infinitesimal surface strain and $\varepsilon_s \approx \lambda_s - 1 << 1$. The surface and bulk materials parameters can be combined to define three characteristic lengths. The elastocapillary length $l_c = \sigma_0 / E$, defines a length scale such that for distances less than it surface stress dominates over elasticity. The length $l_B = B/E$, defines a size of the solid such that bulk and surface extensional strain energy due to some strain are about the same. Finally, the ratio of bending modulus of the surface and Young's modulus of the substrate, $l_k = (k_b / E)^{1/3}$ denotes, for example, the wavelength of a sinusoid on the sample surface for which bending and bulk energies are of about the same magnitude. We note that Eqs (5,6) can apply pointwise, i.e., the materials parameters can be functions of position along the surface.

The nonlinear surface constitutive behavior, and coupling between surface stretching and bending, and between the surface and the bulk material made it necessary to seek numerical solutions. Our model for surface elasticity has been implemented as a surface element for use with the commercial finite element package, ABAQUS® (Fig 3 – details of the implementation are discussed in *ESI*.)

3.4. UV-OZONE TREATED PDMS

We now turn to the third material system, the UVO-treated patterned PDMS samples. UVO treatment creates a thin partially oxidized surface layer without altering the bulk PDMS properties.[38-39] Fig. 5*A* shows typical line scans for this sample set and Fig. 5*B* shows how amplitude depends on surface stretch. Also shown for comparison are the line scan (Fig. 5A) and amplitude (Fig. 5B) of the untreated PDMS control. We observed that for UVO treated PDMS,

(i) the amplitude was distinctly smaller than that of the control ($\frac{a}{a_m} < 0.9$ for the unstretched case), (ii) amplitude decreased significantly with stretch ($\frac{a}{a_m} \sim 0.7$ for a in-plane stretch of ~1.15), and (iii) while the overall deformed shape was rounded, at the upper corners it remained sharp (as indicated by the large grey circles in Fig. 5A and Fig 5D). While there is a discrepancy between the simulated and experimental results in the untreated PDMS sample, it is small compared to the changes in amplitude reported in Figure 5 between untreated and treated PDMS.

That the amplitude was reduced by more than 10% compared to the control suggests that a tensile surface stress is developed due to UVO treatment. This was expected because oxidation of the PDMS surface is known to result in its shrinkage.[38-39] The fact that amplitude further decreased significantly with stretch implies that the surface stress increases with stretch, i.e., the surface had extensional elasticity. This, too, is consistent with the known fact that UVO treatment results in a thin surface layer with significantly higher elastic modulus than the underlying PDMS. [38-39] The fact that corners remain sharp suggests enhanced bending rigidity in that region. That is, it appears that there exists a sufficiently large bending stiffness at the corners such that the local angle is maintained and that surface properties vary with location *s*, the arc length along the sample line scan.

In order to examine systematically the role of surface stress, extensional elasticity, and bending elasticity in predicting the deformed shape, we analyzed three models:

(1) Constant surface stress model: $\sigma_0(s)$ was independent of *s* while $B(s) = k_b(s) = 0$;

(2) Stretch-dependent surface stress model: $\sigma_0(s)$ and $B(s)$ were independent of *s* while $k_b(s) = 0$;

(3) Model with surface stress and bending: $\sigma_0(s)$, $B(s)$ and $k_b(s)$ were spatially non-uniform and non-zero.

First, we made FEM predictions about the amplitude change versus stretch for each model. In order to make the results comparable, we forced the normalized amplitude at zero stretch to be the same for all the models. As shown in Fig. 3*B*, we could immediately rule out the constant surface stress model; its predicted dependence of amplitude on surface stretch was too weak to explain the data. The surface constitutive model must have significant extensional elasticity (but need not have bending) to fit the amplitude data satisfactorily (Fig. 5*B*; $\sigma_0 = 3.25$ N/m; $B = 25$

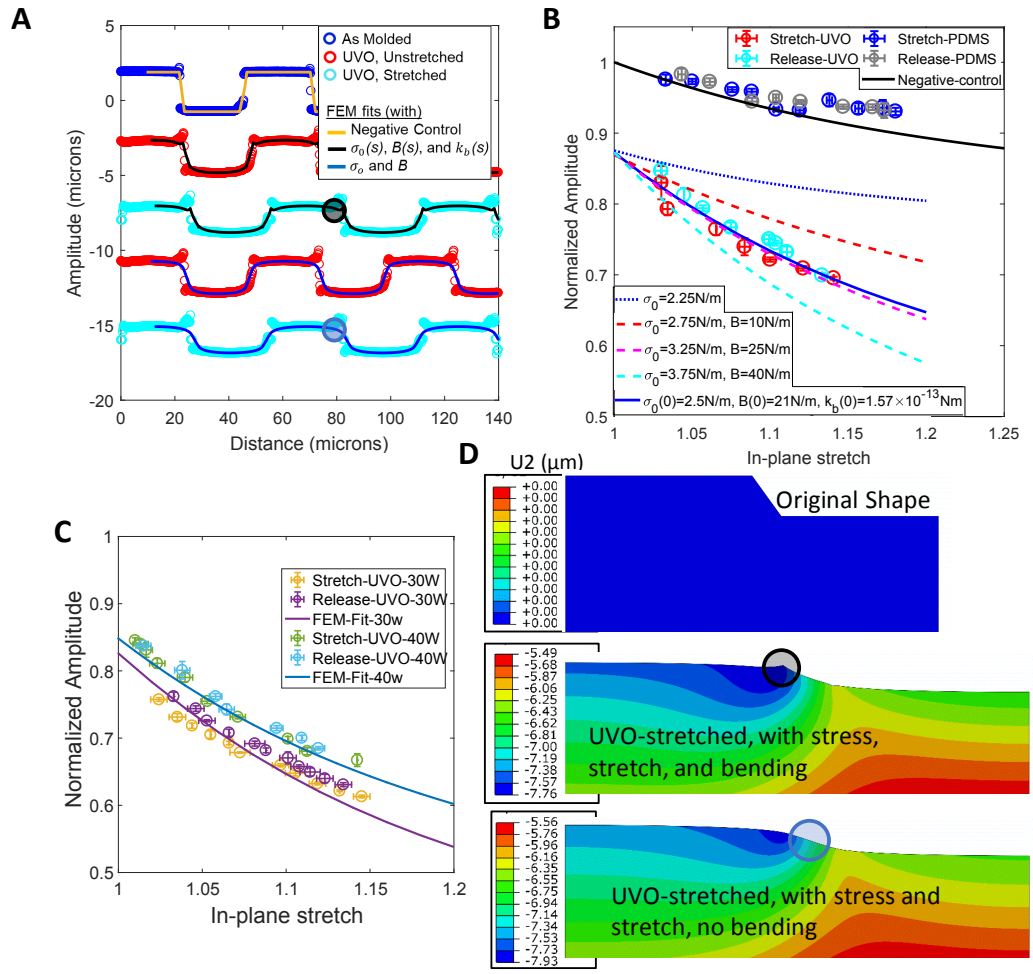

Figure 5. Results of stretching experiments for patterned PDMS samples exposed to UVO for 60 minutes with amplitude a = 1.35 μm and wavelength w = 30 μm, 40 μm, and 50μm (**A**) Typical line scans for a = 1.35 μm and w = 50 μm. The line scan for a sample before UVO exposure shows that the top of the ridge, as molded, is flat. After UVO exposure, the amplitude reduces, the shape overall is rounded, but retains a sharp edge near upper corners (gray circle). (**B**) Normalized amplitude as a function of in-plane stretch for a = 1.35 μm and w = 50 μm. The data are fit by FEM results under various assumptions: constant surface stress model, stretch-dependent surface stress model, and the surface stress-bending coupling model. For the surface stress-bending coupling model, σ_0,B, and k_b values indicated are at s = 0. (**C**) Using the same parameters as for w = 50 microns, we are able to match normalized amplitude for samples with w = 30 μm and 40 μm (line scans are given in Figs. S9*A*, *B*). (**D**) Contours of FEM computed vertical displacement.

N/m). These values of surface stress and extensional elasticity are large compared to those generally found for soft materials – those are rarely larger than 0.1 N/m (*18*). This was not unexpected here because the UVO treatment creates a near-surface silicaceous region that is much greater in stiffness than the untreated PDMS itself.

However, if we also compared the predicted line scan, it was clear that a stretch-dependent surface stress model alone could not capture the deformed shape at the corners without the inclusion of bending, even though it matched the line scan well elsewhere (Fig. 5*A*). To systematically and consistently account for both bending and stretch of the surface, we assumed that exposure to UVO creates a surface region with some characteristic finite thickness $h(s)$, governed by diffusion-limited oxidation of the surface, i.e., the growth of the oxidized layer is controlled by the diffusion of gaseous reactive species into PDMS[38-39]. We expect this layer not to vary in thickness across the surface except in the region where ridges and channels transition from one to the other, because the diffusion profile is inhomogeneous near corners (see *ESI* for more details). This causes surface stress, extensional elasticity and bending modulus to vary with *s*. In flat regions of the sample surface, i.e., far from the corners in its line scan, the thickness has some value $h(0)$, but near the corners it depends on location *s*. In particular, we anticipated that the surface region is thicker near the upper corners. The local values of surface stress, extensional elasticity, and bending modulus are then consistently related to $h(s)$ by

$$\begin{aligned} \sigma_0(s) &= \tau_o\, h(s) \\ B(s) &= E_o h(s) \\ k_b(s) &= E_o \frac{\left[h(s)\right]^3}{12} \end{aligned} \tag{7}$$

where τ_o is the residual stress in the modified surface layer and E_o is its bulk Young's modulus. That is, the surface properties σ_o, B, k_b could be described in terms of $\tau_o, h(s), E_o$. The function $h(s)$ was obtained by solving a diffusion problem that required specification of *Dt*, the product of diffusion coefficient and time. Details are given in *ESI*.

We first fit the UVO treated 50-micron PDMS sample. The parameters used are listed in Table 1 and results are shown in Figs. 5*A* and *B*. Using the same parameters, we then tested whether the model could predict data on samples with different wavelength (40 and 30 microns), Fig. 5*C* (see also Figs. S9*A*, *B*). This test of the model is therefore more stringent than that shown in Fig. 5B. We find an estimate of $E_0 \approx 70\ MPa$ for all samples, which is within the range reported in previous studies of PDMS treated with UVO for 1 h.[45] The value of $h(0) = 300 - 360\ nm$ is also similar to thicknesses previously reported.[38] Finally, we set the bulk residual stress τ_o in the surface layer to have about the same value close to 8 MPa for all samples.

Table 1. Geometry information and fitting parameters for different samples

w (μm)	θ (degrees)	Dt (μm^2)	E_o (MPa)	$h(0)$ (μm)	$\sigma_0(0)$ (N/m)	τ_o (MPa)
50	126	61	70	0.30	2.5	8.3
40	131	61	70	0.31	2.5	8.1
30	120	61	70	0.36	2.8	7.6

4. CONCLUSIONS

In this work, we showed that UVO treatment of PDMS creates a complex surface with significant surface stress *as well as* surface extensional and bending elasticity. We investigated the response of three soft material systems, each with a molded surface pattern comprising shallow ridge-channel geometries, under the influence of surface stress and remote uniaxial stretch.

Two of the systems served as controls: untreated PDMS as a negative control in which the surface plays a negligible role in the material's response and a Gelatin organogel for which a constant, homogeneous, and isotropic surface stress suffices to quantitatively model the deformation. The third system consisted of samples initially identical to the patterned PDMS but with surface modified by UVO treatment, which affects properties upto a characteristic depth of at most a few hundred nm.[38-39] The relevant length scale for flattening driven by surface stress is the periodic spacing of the surface pattern, w, which is much larger than this depth. Therefore, the modified layer can be accurately represented by a 2D surface, as also justified *a posteriori* by our ability to match experimental measurements. In general, surface quantities such as surface energy and surface stress are defined as an excess compared to their homogeneous values far from the interface.[46] Again, this definition, which we have adopted implicitly, is valid when the surface layer thickness is small compared to characteristic length scales in the problem, as is true in our case.

We proposed an elastic free energy function for the surface that contains terms representative of the residual surface stress, surface extensional and bending elasticity. The model was implemented as a surface finite element and used to conduct FEM simulations to model the experiments, and to determine which of the surface properties – surface stress, bending, and surface elasticity – matter, and thus to extract the values of the parameters that represent each. The characteristic length scale of interest is set by the periodic spacing of our surface structures (30-50 microns), for which the choice of a continuum model solved by finite element methods is well-suited. Bulk parameters such as the PDMS shear modulus were measured independently. (Coarse-grained molecular simulations have been used successfully to study surface dominated phenomena at smaller length-scales in the tens of nm.)[15, 22]

The negative control exhibited no deformation on demolding from its master, and small change in amplitude upon stretching the sample. The gel changed its shape significantly compared to that of its mold but the amplitude did not change much upon subsequent stretching. The change in shape of the surface could be modeled as due to the action of an isotropic, homogenous, and constant surface stress with magnitude of about ~70 mN/m. There was no need in this system to invoke extensional or bending elasticity.

The UVO-treated PDMS showed significant change in shape even with little stretch, clearly indicating the presence and influence of surface stress. Unlike the first two sample types, on subsequent stretching the amplitude further decreased significantly, suggesting a stretch-dependent increase in surface stress, i.e., surface extensional elasticity. The reaction of the ozone with the PDMS surface creates a layer with residual stress – this translates into the surface stress. It also endows the surface with extensional elasticity. Because the surface properties are set-up by diffusion and reaction, they are inhomogeneous near corners. In particular, this inhomogeneity makes the bending rigidity of the near-corner regions significant such that the corners resist rounding off.

The values we obtained: surface stress $\sigma(0) = 2.5$ N/m, extensional elasticity, $B(0) = 21$ N/m, and surface bending stiffness, $k_b(0) = 1.6 \times 10^{-13}$Nm, are all quite large compared to values typically measured for soft materials such as organic and inorganic gels and elastomers. For example, a typical value of surface stress of a soft silicone elastomer is about 25 mN/m and often surface extensional elasticity is negligibly small. [32] As mentioned in the Introduction, Gurtin and Murdoch[30] argued that for a *nominally* homogeneous material surface, the surface extensional moduli would be on the order of bulk elastic moduli (~ 1 MPa in our case) times a surface region thickness of about 1 nm, resulting in surface elastic moduli smaller than 1 mN/m in magnitude and hence usually negligible (see eq. 7).

However, our measured values are consistent with the notion that, in this case, surface properties result from a thin, partially oxidized silicaceous layer. That is, in equation (7), the relevant elastic modulus need not be that of the underlying solid, nor need the thickness of the surface layer be set by molecular dimensions. UVO modification partially oxidizes the material near the surface, increasing its modulus into the 100 MPa range[45] over a thickness that is on the order of hundreds of nm.[38] Thus, by eq. (7), a surface extensional modulus of B=25 N/m is quite reasonable. Similarly, it is well-known that PDMS exposed to UVO shrinks; a shrinkage strain of 0.1 would result in a surface stress of 2-3 N/m. Finally, our reported bending stiffness is consistent with the same thickness and modulus (eq. 7). In fact, values for the surface stress and extensional modulus could easily be much higher. We have observed that longer exposure to UVO (90 minutes instead of 60) results in a higher degree of oxidation and higher surface stress sufficient to cause cracking upon stretch. (It is for this reason that we chose the 60-minute UVO exposure duration.) Also, oxygen plasma exposure causes more aggressive and complete oxidation, which was the reason we chose UVO instead. Recall that pure silica has a modulus of about 70 GPa so, with a surface-layer thickness of only 2 nm, we would obtain a surface elastic modulus of 140 N/m; a residual strain of 0.05 would result in a surface stress of 7 N/m.

Thus, we have demonstrated an example of a material with an elastic surface whose description needs to include surface stress, surface extensional elasticity, and surface bending. We have shown that modified surfaces of soft solids can have very large surface stress and elasticity parameters compared to their values for a nominally homogeneous material. By implementing the model as a surface finite element, we have also demonstrated how it can be incorporated into FEM computations for arbitrarily large deformations.

Finally, we consider again the different length scales in this problem. Taking the change in amplitude a / a_m as the primary dependent variable, dimensional analysis demonstrates that

$$\frac{a}{a_m} = f\left(\lambda, \frac{a_m}{w}, \frac{l_c}{w}, \frac{l_B}{w}, \frac{l_k}{w}\right)$$

where f is a dimensionless function of its dimensionless arguments. In experiments, the amplitude decreases with increasing in-plane stretch λ. Fig. 4B shows the change in amplitude in the absence of surface effects is modest, a 5% reduction at $\lambda \approx 1.15$ (a 15% strain). The second dimensionless argument, a_m / w, represents the geometrical feature of the shallow surface ridge-channel patterns. In all our experiments and simulations this ratio is less than 5%, and should not affect the normalized amplitude change (see, for example, eq. 3). The last three dimensionless parameters represent the effects of different characteristic lengths introduced by surface stress, extensional elasticity, and bending elasticity, respectively. In our UVO-PDMS experiments, $l_c \approx 1.3$ μm, $l_B \approx 12$ μm and $l_k \approx 0.43$ μm. The elastocaplliary length l_c is small but still significant in comparison with the wavelength *w*. From this we can expect moderately significant shape change in the absence of stretch, as observed. The surface extensional elasticity induced length l_B is about ten times the elastocapillary length l_c. Thus we expect that for surface stretches of about 1.1 the additional rounding and flattening of the surface will be equivalent to that obtained due to the zero-stretch surface stress. This is consistent with this results of Figs 5B,C. Finally, for our samples, $l_k / w \approx 0.01$, implying that it is negligible for sinusoids with our primary wavelength, and surface bending should dominate only near the corners. Specifically, the corners remain sharp due to this local surface bending rigidity.

We believe that our work offers the first direct demonstration of a complex soft solid surface with significant surface extensional and bending elasticity in addition to surface stress. It is not typical to see these three properties in conjunction in solids. It is analogous to the behavior of complex aqueous liquid systems with surfactants such as lipids, termed Gibbs elasticity. Soft solids have long been used as gels, rubbers, adhesives, and are finding many new applications such as in soft robotics and biomaterials such as for wound healing. Design for mechanical functionality with soft materials require quantitative understanding of how they respond to deformation. There is a particular need to understand the role of the surface as a mechanical element and the work we have presented establishes a class of elastic surfaces that have not been well understood despite extensive use of them in various applications.

5. CONFLICTS OF INTEREST

There are no conflicts to declare.

6. ACKNOWLEDGEMENTS

This work was supported by the U.S. Department of Energy, Office of Basic Energy Sciences, Division of Materials Sciences and Engineering under award DEFG02-07ER46463 (to AJ and CYH). SY acknowledges partial supported by NSF/Emerging Frontiers in Research and Innovation–Origami Design for Integration of Self-Assembling Systems for Engineering Innovation (EFRI-ODISSEI) Grant 13-31583. We are grateful to Ms. Hye-Na Kim for assistance with the UV-Ozone treatment, to Ms. Avani Pisapati for assistance with experiments, to Dr. Robert Style for helpful discussion, and to Professor K. Schultz for the use of the rheometer.

7. REFERENCES

1. Adamson, A. W.; Gast, A. P., *Physical Chemistry of Surfaces*. John Wiley & Sons: New York, 1997.
2. Rowlinson, J. S.; Widom, B., *Molecular Theory Of Capillarity*. Oxford University Press: New York, USA, 1989.
3. deGennes, P.-G.; Brochard-Wyart, F.; Quere, D., *Capillarity and Wetting Phenomena. Drops, Bubbles, Pearls, Waves*. Springer Science+Business Media, Inc.: New York, 2002.
4. Hui, C.-Y.; Jagota, A.; Lin, Y. Y.; Kramer, E. J., Constraints on Micro-Contact Printing Imposed by Stamp Deformation", . *Langmuir* **2002,** *18*, 1394-1404.
5. Style, R. W.; Jagota, A.; Hui, C.-Y.; Dufresne, E. R., Elastocapillarity: Surface tension and the mechanics of soft solids. *Annual Review of Condensed Matter Physics* **2017,** *8*, 99-118.
6. Nicolson, M. M., Surface Tension in Ionic Crystals. *Proceedings OF THE ROYAL SOCIETY A-MATHEMATICAL PHYSICAL AND ENGINEERING SCIENCES* **1955,** *228* (1175), 490-510.
7. Josell, D.; Spaepen, F., Determination of the interfacial tension by zero creep experiments on multilayers—II. Experiment. *Acta metallurgica et materialia* **1993,** *41* (10), 3017-3027.
8. Robert C. Cammarata, K. S., Surface and Interface Stresses. *Annual Review of Materials Science* **1994,** ***24***, 214-234.
9. Cammarata, R.; Sieradzki, K., Effects of surface stress on the elastic moduli of thin films and superlattices. *Physical review letters* **1989,** *62* (17), 2005.
10. Berger, R.; Delamarche, E.; Lang, H. P.; Gerber, C.; Gimzewski, J. K.; Meyer, E.; Güntherodt, H.-J., Surface stress in the self-assembly of alkanethiols on gold. *Science* **1997,** *276* (5321), 2021-2024.
11. Mora, S.; Phou, T.; Fromental, J.-M.; Pismen, L. M.; Pomeau, Y., Capillarity Driven Instability of a Soft Solid. *Physical Review Letters* **2010,** *105* 214301.
12. Mora, S.; Maurini, C.; Phou, T.; Fromental, J.-M.; Audoly, B.; Pomeau, Y., Solid drops: Large capillary deformations of immersed elastic rods. *Physical Review Letters* **2013,** *111* (11), 114301.
13. Paretkar, D.; Xu, X.; Hui, C.-Y.; Jagota, A., Flattening of a patterned compliant solid by surface stress. *Soft Matter* **2014,** *10* (23), 4084-4090.
14. Johnson, K. L., *Contact Mechanics*. Cambridge University Press: Cambridge, 1985.
15. Carrillo, J.-M. Y.; Dobrynin, A. V., Contact mechanics of nanoparticles. *Langmuir* **2012,** *28* (29), 10881-10890.
16. Style, R. W.; Hyland, C.; Boltyanskiy, R.; Wettlaufer, J. S.; Dufresne, E. R., Surface tension and contact with soft elastic solids. *Nature communications* **2013,** *4*.
17. Salez, T.; Benzaquen, M.; Raphaël, É., From adhesion to wetting of a soft particle. *Soft Matter* **2013,** *9* (45), 10699-10704.
18. Xu, X.; Jagota, A.; Hui, C.-Y., Effects of surface tension on the adhesive contact of a rigid sphere to a compliant substrate. *Soft Matter* **2014,** *10* (26), 4625-4632.
19. Hui, C.-Y.; Liu, T.; Salez, T.; Raphael, E.; Jagota, A., Indentation of a rigid sphere into an elastic substrate with surface tension and adhesion. *Proceedings of the Royal Society of London A: Mathematical, Physical and Engineering Sciences* **2015,** *471*, 20140727.
20. Jerison, E. R.; Xu, Y.; Wilen, L. A.; Dufresne, E. R., Deformation of an Elastic Substrate by a Three-Phase Contact Line. *Physical Review Letters* **2011,** *106* (18), 186103.
21. Marchand, A.; Das, S.; Snoeijer, J. H.; Andreotti, B., Contact angles on a soft solid: from Young's law to Neumann's law. *Physical Review Letters* **2012,** *109* (23), 236101.
22. Cao, Z.; Dobrynin, A. V., Polymeric Droplets on Soft Surfaces: From Neumann's Triangle to Young's Law. *Macromolecules* **2015,** *48* (2), 443-451.
23. Hui, C.-Y.; Jagota, A., Planar equilibrium shapes of a liquid drop on a membrane. *Soft Matter* **2015**.

24. Nadermann, N.; Hui, C.-Y.; Jagota, A., Solid surface tension measured by a liquid drop under a solid film. *Proceedings of the National Academy of Sciences* **2013,** *110* (26), 10541-10545.
25. Schulman, R. D.; Dalnoki-Veress, K., Liquid Droplets on a Highly Deformable Membrane. *Physical Review Letters* **2015,** *115* (20), 206101.
26. Mondal, S.; Phukan, M.; Ghatak, A., Estimation of solid–liquid interfacial tension using curved surface of a soft solid. *Proceedings of the National Academy of Sciences* **2015,** *112* (41), 12563-12568.
27. Vella, D.; Adda-Bedia, M.; Cerda, E., Capillary wrinkling of elastic membranes. *Soft Matter* **2010,** *6* (22), 5778-5782.
28. Fuller, G. G.; Vermant, J., Complex fluid-fluid interfaces: rheology and structure. *Annual review of chemical and biomolecular engineering* **2012,** *3*, 519-543.
29. Shuttleworth, R., The Surface Tension of Solids. *Proceedings of the Physical Society. A* **1950,** *63* (5), 444.
30. Gurtin, M. E.; Ian Murdoch, A., Surface stress in solids. *International journal of solids and structures* **1978,** *14* (6), 431-440.
31. Steigmann, D.; Ogden, R. In *Elastic surface—substrate interactions*, Proceedings of the Royal Society of London A: Mathematical, Physical and Engineering Sciences, The Royal Society: 1999; pp 437-474.
32. Xu, Q.; Jensen, K. E.; Boltyanskiy, R.; Sarfati, R. e.; Style, R. W.; Dufresne, E. R., Direct Measurement of Strain-dependent Solid Surface Stress. *arXiv preprint arXiv:1702.00684* **2017**.
33. Helfrich, W., Elastic properties of lipid bilayers: theory and possible experiments. *Zeitschrift für Naturforschung C* **1973,** *28* (11-12), 693-703.
34. Kusumaatmaja, H.; Li, Y.; Dimova, R.; Lipowsky, R., Intrinsic contact angle of aqueous phases at membranes and vesicles. *Physical review letters* **2009,** *103* (23), 238103.
35. Milner, S.; Joanny, J.; Pincus, P., Buckling of Langmuir monolayers. *EPL (Europhysics Letters)* **1989,** *9* (5), 495.
36. Stafford, C. M.; Harrison, C.; Beers, K. L.; Karim, A.; Amis, E. J.; VanLandingham, M. R.; Kim, H.-C.; Volksen, W.; Miller, R. D.; Simonyi, E. E., A buckling-based metrology for measuring the elastic moduli of polymeric thin films. *Nature materials* **2004,** *3* (8), 545-550.
37. Lin, P.-C.; Vajpayee, S.; Jagota, A.; Hui, C.-Y.; Yang, S., Mechanically tunable dry adhesive from wrinkled elastomers. *Soft Matter* **2008,** *4* (9), 1830-1835.
38. Mills, K.; Zhu, X.; Takayama, S.; Thouless, M., The mechanical properties of a surface-modified layer on polydimethylsiloxane. *Journal of materials research* **2008,** *23* (1), 37-48.
39. Efimenko, K.; Wallace, W. E.; Genzer, J., Surface modification of Sylgard-184 poly (dimethyl siloxane) networks by ultraviolet and ultraviolet/ozone treatment. *Journal of colloid and interface science* **2002,** *254* (2), 306-315.
40. Glassmaker, N. J.; Jagota, A.; Hui, C. Y.; Noderer, W. L.; Chaudhury, M. K., Biologically inspired crack trapping for enhanced adhesion. *Proceedings of the National Academy of Sciences of the United States of America* **2007,** *104* (26), 10786.
41. Hourlier-Fargette, A.; Antkowiak, A.; Chateauminois, A.; Neukirch, S., Role of uncrosslinked chains in droplets dynamics on silicone elastomers. *Soft Matter* **2017,** *13* (19), 3484-3491.
42. Green, A. E.; Naghdi, P. M.; Wainwright, W., A general theory of a Cosserat surface. *Archive for Rational Mechanics and Analysis* **1965,** *20* (4), 287-308.
43. Simo, J. C.; Fox, D. D.; Rifai, M. S., On a stress resultant geometrically exact shell model. Part III: Computational aspects of the nonlinear theory. *Computer Methods in Applied Mechanics and Engineering* **1990,** *79* (1), 21-70.
44. Gao, X.; Huang, Z.; Qu, J.; Fang, D., A curvature-dependent interfacial energy-based interface stress theory and its applications to nano-structured materials:(I) General theory. *Journal of the Mechanics and Physics of Solids* **2014,** *66*, 59-77.

45. Hillborg, H.; Tomczak, N.; Olàh, A.; Schönherr, H.; Vancso, G. J., Nanoscale hydrophobic recovery: A chemical force microscopy study of UV/ozone-treated cross-linked poly (dimethylsiloxane). *Langmuir* **2004,** *20* (3), 785-794.
46. Nozieres, P.; Wolf, D., Interfacial properties of elastically strained materials. *Zeitschrift für Physik B Condensed Matter* **1988,** *70* (3), 399-407.

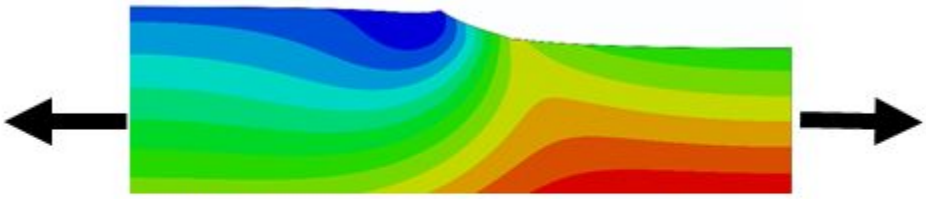

UVO-Treated PDMS has Surface Stress, Extensional, and Bending Elasticity.